

## Accepted Manuscript

Nano-structured morphological features of pulsed direct current magnetron sputtered Mo films for photovoltaic applications

Sreejith Karthikeyan, Arthur E. Hill, Richard D. Pilkington

PII: S0040-6090(11)01456-8  
DOI: doi: [10.1016/j.tsf.2011.07.069](https://doi.org/10.1016/j.tsf.2011.07.069)  
Reference: TSF 29676

To appear in: *Thin Solid Films*

Received date: 15 March 2011  
Revised date: 6 July 2011  
Accepted date: 27 July 2011



Please cite this article as: Sreejith Karthikeyan, Arthur E. Hill, Richard D. Pilkington, Nano-structured morphological features of pulsed direct current magnetron sputtered Mo films for photovoltaic applications, *Thin Solid Films* (2011), doi: [10.1016/j.tsf.2011.07.069](https://doi.org/10.1016/j.tsf.2011.07.069)

This is a PDF file of an unedited manuscript that has been accepted for publication. As a service to our customers we are providing this early version of the manuscript. The manuscript will undergo copyediting, typesetting, and review of the resulting proof before it is published in its final form. Please note that during the production process errors may be discovered which could affect the content, and all legal disclaimers that apply to the journal pertain.

## Nano-structured morphological features of pulsed direct current magnetron sputtered Mo films for photovoltaic applications.

Sreejith Karthikeyan<sup>\*</sup>, Arthur E Hill and Richard D Pilkington

Materials and Physics Research Centre, University of Salford, The Crescent, Salford, M5 4WT, UK

<sup>\*</sup>Corresponding author: s.karthikeyan@edu.salford.ac.uk

### Abstract

Historically, molybdenum thin films have been used as the back contact for Cu(In,Ga)Se<sub>2</sub> based solar cells and as such the properties of these layers play an important role in the overall cell structure. This paper describes the production of molybdenum films using pulsed d.c magnetron sputtering from compressed molybdenum powder targets. The films were deposited at different substrate temperatures under constant power and constant current modes, and analysed using X-ray diffraction, scanning electron microscopy, atomic force microscopy and four point resistance probe. Mechanical strain and resistivity were found to decrease with substrate temperature together with a shift in the (110) crystallographic plane towards higher diffraction angles. All films were well adhered to the glass substrates irrespective of their high tensile strain. Surface morphology analysis revealed the presence of nano-structured stress relief patterns which can enhance the nucleation sites for subsequent CuInSe<sub>2</sub> deposition. A high-resolution cross sectional image showed the columnar growth of the films. Surface roughness analysis revealed that roughness increased with increase in substrate temperature.

### Keywords

Molybdenum films, Pulsed D.C. Magnetron Sputtering, nano-structured stress relief pattern, powder sputtering, back contact layer.

## 1. Introduction

A typical CuInSe<sub>2</sub> (CIS) or Cu(In,Ga)Se<sub>2</sub> (CIGS) based solar cell comprises a glass/Mo/(CIS/CIGS)/CdS/i-ZnO/ZnO heterojunction with the molybdenum film being used as a back contact layer [1]. The reason is partially historic and partly scientific [2]. A good back electrode should provide an ohmic contact with the p-type absorbing layer, have low resistivity and be well adhered to the glass substrate. Other back contacts such as W, Mo, Cr, Ta, Nb, V and Mn have been tried, but it has been shown that Mo back contact based solar cells had superior efficiency and reproducibility [3]. In solar cell applications, the Mo electrode forms an ohmic contact via an intermediate MoSe<sub>2</sub> layer [3-5]. Wada *et al.* believe that the MoSe<sub>2</sub> formation is aided by the diffusion of Na from the soda lime glass substrate into both the CIGS and the Mo layers [5]. Researchers have developed a variety of techniques for depositing such Mo layers. Sputtering is considered as one of the most important of these because it offers control over the different operating parameters and the ability to produce uniform layers with high reproducibility rates compared to other techniques such as thermal evaporation. Mo films in the past have been traditionally produced by d.c sputtering [2-4] or r.f sputtering [6] from a solid target. Various commercial industries such as Shell Solar, Würth Solar, Global Solar, Nanosolar, Ascent Solar, etc.. use sputtered Mo films on various substrates such as glass, steel or flexible polymer as a back contact for CIGS based solar cells [7]. This work describes the deposition of Mo films by pulsed d.c. magnetron sputtering (PDMS) using a powder target. The powder sputtering technique is a widely accepted method for depositing dielectric materials and for the reactive sputtering of aluminium oxide, zinc oxide etc.[8, 9]. During magnetron sputtering the magnets, which are placed behind the target, produce electrons that are more confined near the target surface. This leads to an increase in sputtering rate. However, target utilization is reduced because the non-uniform distribution of magnetic fields leads to

enhanced erosion from the target , causing localized thinning of the target and producing a "race track" pattern [10]. The race track will eventually penetrate through the target and can cause sputtering of the target holder material. The usage of a powder target can reduce the material wastage associated with this race track effect which limits the effective target area. Molybdenum metal is produced by the powder metallurgy techniques in which Mo powder is hydrostatically compacted and sintered at about 2100°C [11]. This material must then be cut into the shape required for the solid target. The use of powder can cut out this intermediate process and save production costs. Hence the use of powder target increases the material utilisation and reduces production cost in large scale. Pulsed d.c magnetron sputtering from powder target also produced stoichiometric CuInSe<sub>2</sub> from single step process this layer is subsequently deposited on top of Mo layer [12].

The deposited Mo films had low resistivity, were pin hole free and adhered well to the glass substrates. Scofield et al,[2] reported a problem associated with the adhesion of Mo films on glass substrates at low argon sputtering pressures. These results are not only dependent on the pressure but also depend on the system geometry and configuration. In our case we have deposited films at the lowest pressure possible ( $7.0 \times 10^{-1}$  Pa) and they were found to be well adhered to the glass substrate. A range of work has been reported on the stress/strain related issues of films and their mechanical and electrical behaviour following deposition by the normal d.c sputtering method [2, 13-17]. There have been no studies conducted on the effect of stress or strain in pulsed d.c. magnetron sputtered films, especially from powdered targets. The Mo thin films sputtered using ordinary d.c. [2, 18] and r.f.[6] magnetron sputtering at low pressure were found to have compressive strain and showed low resistivity but our pulsed d.c. sputtered Mo films were found to have very high tensile strain with relatively high resistivity. The resistivity was reduced to a lower value suitable for solar cell applications following heat treatment. These preliminary results

require further research to optimise the magnetron operating parameters and hence the film characteristics, such as the resistivity.

## 2. Experimental Details

The system consisted of a cylindrical stainless steel chamber evacuated with a turbo molecular high vacuum pump backed by a rotary pump. A detailed description of the system is described in our previous paper [19]. Molybdenum powder of >99.9% purity (Sigma Aldrich) with a particle size of 1-2 $\mu\text{m}$  was used as the target source. The powder was compressed into a 5 cm diameter recess in the target head as shown in Figure 1. The system was pumped to a base pressure of  $5.0 \times 10^{-4}$  Pa. The deposition was performed in an argon atmosphere regulated by a mass flow controller. The minimum pressure for a plasma discharge was found to be  $6.0 \times 10^{-1}$  Pa but to obtain stable plasma conditions a minimum pressure of  $7.0 \times 10^{-1}$  Pa was used. The films were deposited at substrate temperatures ranging from 47  $^{\circ}\text{C}$  (no substrate heating) to 300  $^{\circ}\text{C}$  onto soda lime glass which had been cleaned with isopropyl alcohol and acetone in an ultrasonic bath and dried with an argon gas blower.

The films' thickness was measured using a Dektac<sup>3</sup> ST surface profilometer and the resistivity was measured by the four point probe method. The structural properties were investigated using a Simens D 5000 X-ray diffractometer with Cu  $K\alpha$  radiation ( $\lambda=0.154\text{nm}$ ). The powder was analysed using locked coupled mode ( $2\theta$  from 10 to 90) and the films were analysed using a detector scan ( $2\theta$  from 10 to 60). The morphological properties were analysed by a Philips XLS -30 field emission gun scanning electron microscope (SEM) and a Digital Instruments Nanoscope III atomic force microscope (AFM). The SEM was operated in 400000x magnification in ultra high resolution mode with an operating voltage of 10 kV. The AFM analysis was performed with a Veeco RTESPA tip (300 kHz) in tapping mode. The AFM analysis was used to determine the

roughness of the films. A “Scotch tape” test was conducted to study the adhesion properties of the films on the glass substrates using tape stuck onto a rectangular scratched area of approximately 1cm x 1cm.

### 3. Results and Discussion

#### 3.1. Target Powder

X-ray diffraction (in locked coupled mode;  $2\theta$  from 10 to 90 degree) was used to ascertain structural properties of the Mo powder, Figure 2. The spectrum matched that reported by JCPDS CAS Number 42-1120 for molybdenum samples. Four prominent peaks corresponding to the (110), (200), (211) and (220) planes were present. This suggests that the powder is in body-centred cubic phase. The preferred orientation was in the (110) plane.

#### 3.2. Mo films at different substrate temperatures deposited under constant power

##### 3.2.1. Operating parameters, thickness, and resistivity results

The films were deposited at different substrate temperatures, starting with no external heating, up to a maximum of 300 °C. The PDMS power supply was set to constant power mode (50W  $\pm$  5%) with a frequency of 75kHz and a pulse off time  $\tau_{\text{off}}$  of 0.5 $\mu$ s; the operating pressure was 7.0  $\times 10^{-1}$  Pa and the sputtering time was 90 minutes. Results for film thickness ( $d$ ) and resistivity ( $\rho$ ), given in Table 1, show a reduction in thickness with increased substrate temperature and a corresponding decrease in film resistivity. All films “passed” the adhesion tape test in that the adhesive tape peeled off the films leaving well adhered films on the substrates. The resistivity of the films deposited using this method is high compared to that obtained by d.c sputtering from a solid target [2], however the resistivity is reduced to a lower value with increase in substrate temperature.

##### 3.2.2. Structural analysis

X-ray analysis of the films revealed a preferred (110) crystallographic orientation matching that of the starting powder. (Figure 3) suggesting that the films were in body-centred cubic

Im3m phase (JCPDS 42-1120). The accurate  $2\theta$  values were determined from the diffraction data using a standard Lorentzian function. A clear shift in  $2\theta$  towards higher angles was noticed ( $39.65^\circ$  to  $40.38^\circ$ ) with an increase in substrate temperature. These values were low compared to the JCPDS value of  $40.516^\circ$ . The lattice spacing  $d_{110}$  was determined using Bragg's law. The lattice parameter was determined using this  $d$  space value. The strain in the films was calculated using the following equation.

$$\text{Strain}\% = \frac{a - a_0}{a_0} \times 100 \quad (1)$$

where  $a$  is the calculated lattice parameter and  $a_0$  is the reference lattice constant  $3.1469 \text{ \AA}$  (JCPDS 42-1120). This parameter gives a clear picture of whether the strain in the film is tensile or compressive. The calculated values of  $2\theta$  and strain percentage are shown in Figure 4.

The strain analysis revealed that the films were under tensile strain [13] and that the strain percentage reduced with increase in temperature. There are several factors that can contribute to the origin of this strain profile, e.g. voids, oxygen or argon impurities and crystallographic flaws[13]. These in turn are dependent on operating parameters such as substrate temperature, sputtering gas species, operating pressure, deposition rate, angle of incidence, apparatus geometry and source-substrate distance[20]. The decrease in strain percentage with increase in substrate temperature suggests that the temperature can control the strain of the films which in turn can control the mechanical, electrical and optical properties [13]. The work reported by Thornton and Hoffman suggests that the substrate temperature ( $T_s$ ) and the melting point of the coating material ( $T_m$ ) are important to the stress related material characteristics and they suggest that it is particularly important for materials having a low melting point, such as aluminium[20]. Increasing the  $T_s/T_m$  ratio can relax the intrinsic stress. Our studies suggest that this is valid for Mo films, which have a high melting point. The increase in temperature reduced the overall strain percentage.

However, there is no reported Mo deposition technique which has resulted in strong adhesion without cracking under a tensile strain percentage  $> 1.0$ . The main concern about high tensile strain or stress in films is that it usually leads to cracking and subsequent peeling off from the substrate [6, 16]. The greater the thickness the greater will be the cracking / peeling off force for a given level of stress. In our case, films with  $> 1.0 \mu\text{m}$  thickness retained their adhesive properties, even eight months after deposition.

The increase in peak intensity at higher temperatures suggests that there is an associated improved crystalline property. The Lorentzian fits revealed that the Full Width Half Maxima (FWHM) of the samples decreased with increase in temperature. The crystalline sizes of the molybdenum films were calculated using the Debye-Scherrer equation:

$$L = \frac{k\lambda}{\beta \cos \theta} \quad (2)$$

Where  $L$  is the particle size,  $k$  is the Debye-Scherrer constant (0.9),  $\theta$  is the Bragg angle and  $\beta$  is the Full Width Half Maximum which is determined from the following equation.

$$\beta^2 = B^2 - b^2 \quad (3)$$

Where  $B$  is the experimental width calculated from the X-ray diffraction data using the Lorentzian function and  $b$  is the instrument broadening which is determined using a Si standard sample. The FWHM is inversely proportional to the crystalline size. The calculated FWHM and crystalline size are shown in Figure 5, which suggests that the crystalline size increased with increase in temperature. The larger crystal sizes and the reduced strain percentage result in reduced resistivity of the films grown at higher temperatures (Table 1).

### 3.2.3. Surface morphology of Mo films

The surface morphology of the films was analysed using scanning electron microscopy. SEM images of the films deposited with no heating and of films grown at  $150^\circ\text{C}$  are shown in Figure 6.

The SEM images show that there is a drastic change in particle shape from a cluster of small grains to a fibrous, columnar needle-like structure for films grown at 150 °C. A similar sort of pattern was previously reported by Ogawa *et al.* [21]. They named the “wrinkled spot” and “wavy ride” stress relief patterns observed in ion beam and d.c. magnetron sputtered films, but their patterns were observed in the buckled portion of the films and with fairly large grain sizes  $> 5\mu\text{m}$  in length [21]. These kinds of micrometre-sized patterns were also reported by Wu *et al.* using an optical microscope [16]. The Mo films reported here showed nanometre sized clusters that have nano-structured stress relief patterns. These types of columnar grains and faceted surfaces which were observed at 150 °C were previously reported by Malhotra *et al.* [13] and Al-Thani *et al.* [22]. This patterned growth feature can improve the adhesion of subsequent CIS/CIGS layers in a solar cell. The work done by Al-Thani *et al.* on CIGS solar cells with different morphologically featured Mo back contacts suggests that the devices incorporating such fibrous grains exhibited a higher efficiency. They also observed morphological changes with different operating pressures [22] that match our results. A high-resolution cross sectional image of a film deposited at 150 °C is shown in Figure 7. The cross sectional analysis revealed that the film had columnar growth with closed inter columnar gaps.

The topography of films was also analysed using AFM in tapping mode, (Figure 8) which supports the X-ray diffraction analysis that the grain size increased with increase in temperature. The roughness of the films was analyzed from AFM data using WSxM software [23]. The roughness increased from 4nm to 7nm with the increase in substrate temperature. Small columnar growth units form larger clusters or islands and this process can lead to an increase in the overall roughness of the films at higher temperatures.

### **3.3. Mo films at different substrate temperatures under constant current mode**

#### **3.3.1. Operating parameters, thickness and resistivity results**

Mo films with (110) out-of-plane texture are used in X-ray mirrors and as a back contact in solar cells [13]. In order to investigate the reproducibility of the adherence property of the high strain % Mo films, the tests described above were repeated for films deposited with the power supply set to constant current mode at a value of 0.10A. The frequency was set to 100 kHz and pulse off time was set to 1 $\mu$ S at 9.0 x10<sup>-1</sup> Pa.

The experiments were halted when the strain % dropped to <1.0. The operating parameters, thickness and resistivity measurements are summarised in Table 2. As expected, the resistivity again reduced with increase in substrate temperature during deposition. The important observation is that of thickness which reduced drastically with increase in substrate temperature compared with the constant power mode results. In constant current mode operation we have observed significant fluctuations in the average sputtering voltage as registered on the power supply. This is possibly due to the heating effect near the target surface. This fluctuation was greater at higher substrate temperatures. Real-time-resolved monitoring of the plasma and the temperature near the target would give more information of the processes involved. The preliminary observations suggest that constant power mode is more stable for the deposition of Mo films from powder targets.

### **3.3.2. Structural analysis**

The X-ray diffraction suggests that the Mo films were strongly structured with a preferred (110) plane shown in Figure 9. The diffraction spectra of Mo films deposited under constant current mode are exactly the same as for the films deposited under constant power mode. The shift in 2 $\theta$  values was reproduced. The same models for fitting and analysis were carried out as described before. The crystalline quality improved with increase in substrate temperature.

The 2 $\theta$  and strain % calculated from the (110) peak are shown in Figure 10. The strain % decreased with increase in temperature and the value reduced to unity at 200<sup>0</sup>C. The

FWHM is decreased with increase in temperature. The morphological features were exactly similar to those produced under constant power mode.

### **Conclusion**

Molybdenum films were prepared from powder targets using the pulsed d.c magnetron sputtering technique under both constant power and constant current mode. The XRD analysis revealed that the films were in the body-centred cubic  $Im\bar{3}m$  phase with (110) preferred crystallographic orientation, matching the starting material. Strain analysis was performed from the XRD data and irrespective of the large strain percentage, the films were found to be well adhered to the glass substrates. With increase in substrate temperature it was seen that the strain percentage, resistivity and thickness reduced while the grain size and surface roughness increased. The resistivity was high compared with that reported by others using solid targets but this can be reduced by additional substrate heating. A nano-structured columnar needle like morphological change was observed at higher temperatures. Films deposited under constant power mode showed better thickness reproducibility with temperature compared with films deposited under constant current mode. The relatively low resistivity and good adhesion properties suggest that Mo films deposited from powder targets can be used as well-adhered back contact layers for CIGS based solar cells. This powder deposition process can reduce the cost and material wastage associated with the traditional sputtering process from a solid target. These are the preliminary results; further research is being carried out to study the adhesion properties of the films and to reduce the resistivity by adjusting the operating parameters and changing the target geometry.

### **Acknowledgement**

The authors gratefully acknowledge the Joule Centre for the funding of this project (Grant No: JSGP408/05). Sincere thanks are due to the Higher Education Funding Council for

England (HEFCE) for the award of a research fellowship to Sreejith Karthikeyan under the ORSAS programme.

ACCEPTED MANUSCRIPT

## References

- [1] R.A. Mickelsen, W.S. Chen, *Appl. Phys. Lett.* 36 (1980) 371.
- [2] J.H. Scofield, A. Duda, D. Albin, B.L. Ballard, P.K. Predecki, *Thin Solid Films* 260 (1995) 26.
- [3] K. Orgassa, H.W. Schock, J.H. Werner, *Thin Solid Films* 431-432 (2003) 387.
- [4] R.J. Matson, O. Jamjoum, A.D. Buonaquisti, P.E. Russell, L.L. Kazmerski, P. Sheldon, R.K. Ahrenkiel, *Solar Cells* 11 (1984) 301.
- [5] T. Wada, N. Kohara, S. Nishiwaki, T. Negami, *Thin Solid Films* 387 (2001) 118.
- [6] H. Khatri, S. Marsillac, *J. Phys.: Cond. Matter.* 20 (2008) 055206.
- [7] H.S. Ullal., B.v. Roedem., *Solid State Technology*, vol. 2, 2008, p. 52.
- [8] P.J. Kelly, P.S. Henderson, R.D. Arnell, G.A. Roche, D. Carter, *J. Vac. Sci. Technol., A* 18 (2000) 2890.
- [9] P.J. Kelly, Y. Zhou, *J. Vac. Sci. Technol., A* 24 (2006) 1782.
- [10] Q. Qiu, Q. Li, J. Su, Y. Jiao, J. Finley, *IEEE Transactions on Plasma Science* 36 (2008) 1899.
- [11] H. Walser, J. Shields, John A., *International Molybdenum Association Newsletter*, vol. [http://www.imoa.info/\\_files/newsletter/IMOA\\_Newsletter\\_2007\\_07.pdf](http://www.imoa.info/_files/newsletter/IMOA_Newsletter_2007_07.pdf), 2007, p. 1.
- [12] S. Karthikeyan, A.E. Hill, R.D. Pilkington, J.S. Cowpe, J. Hisek, D.M. Bagnall, *Thin Solid Films* 519 (2011) 3107.
- [13] S.G. Malhotra, Z.U. Rek, S.M. Yalisove, J.C. Bilello, *J. Vac. Sci. Technol., B* 15 (1997) 345.
- [14] D.W. Hoffman, J.A. Thornton, *Thin Solid Films* 45 (1977) 387.
- [15] J.A. Thornton, D.W. Hoffman, *J. Vac. Sci. Technol., A* 14 (1977) 164.
- [16] Y.G. Wu, E.H. Cao, Z.S. Wang, J.M. Wei, W.X. Tang, L.Y. Chen, *Appl. Phys. A: Mater. Sci. Process.* 76 (2003) 147.
- [17] J.M. Freitag, B.M. Clemens, *Appl. Phys. Lett.* 73 (1998) 43.
- [18] P.M.P. Salomé, J. Malaquias, P.A. Fernandes, A.F.d. Cunha, *J. Phys. D: Appl. Phys.* 43 (2010) 345501.
- [19] S. Karthikeyan, A.E. Hill, J.S. Cowpe, R.D. Pilkington, *Vacuum* 85 (2010) 634.
- [20] J.A. Thornton, D.W. Hoffman, *Thin Solid Films* 171 (1989) 5.
- [21] K. Ogawa, T. Ohkoshi, T. Takeuchi, T. Mizoguchi, T. Masumoto, *Jpn. J. Appl. Phys.* 25 (1986) 695.
- [22] A.A.-T. Hamda, F.S. Hasoon, M. Young, S. Asher, J.L. Alleman, M.M. Al-Jassim, D.L. Williamson, *Twenty-Ninth IEEE Photovoltaic Specialist Conference*, 2002, p. 720.
- [23] I. Horcas, R. Fernandez, J.M. Gomez-Rodriguez, J. Colchero, J. Gomez-Herrero, A.M. Baro, *Rev. Sci. Instrum.* 78 (2007) 013705.

**Table Captions.**

Table 1 Thickness and resistivity of samples deposited at different temperature under constant power mode.

Table 2 Thickness and resistivity of samples deposited at different temperatures under constant current mode.

**Figure Captions.**

Figure 1. Powdered molybdenum target.

Figure 2. X-ray diffraction spectrum of molybdenum powder.

Figure 3. X-ray diffraction spectra of Mo films at different substrate temperatures under constant power mode.

Figure 4.  $2\theta$  and strain % values of Mo films deposited at different temperatures under constant power mode (The curves are guides to the eye).

Figure 5. FWHM and Particle Size of Mo films deposited at different temperatures under constant power mode (The curves are guides to the eye).

Figure 6. SEM images of Mo films deposited (a) with no heating (b) at  $150\text{ }^{\circ}\text{C}$  under constant power

Figure 7. High resolution cross sectional image of Mo films deposited at  $150\text{ }^{\circ}\text{C}$ .

Figure 8 AFM images ( $1\mu\text{m} \times 1\mu\text{m}$ ) of Mo films deposited at (a) room temperature (b)  $150\text{ }^{\circ}\text{C}$  (c)  $300\text{ }^{\circ}\text{C}$  under constant power.

Figure 9. X-ray diffraction spectra of Mo films at different substrate temperature under constant current.

Figure 10.  $2\theta$  and strain % values of Mo films deposited at different temperatures under constant current mode (The curves are guides to the eye).

Table 1

Sample Name	Substrate Temperature $^{\circ}\text{C}$	Thickness $d$ nm	Resistivity $\rho$ $\Omega \text{ cm}$	Adhesion Test
Molp200	47	1323	0.002021	Pass
Molp201	100	1315	0.001384	Pass
Molp202	150	1284	0.000763	Pass
Molp203	200	1264	0.000853	Pass
Molp204	250	1248	0.000487	Pass
Molp205	300	1250	0.000256	Pass

Table 2

Sample Name	Substrate Temperature $^{\circ}\text{C}$	Thickness $d$ nm	Resistivity $\rho$ $\Omega \text{ cm}$	Adhesion Test
Mol102	47	1102	0.001810	Pass
Mol201	100	921	0.000991	Pass
Mol202	150	623	0.000555	Pass
Mol203	200	480	0.000227	Pass



Figure 1

ACCEPTED

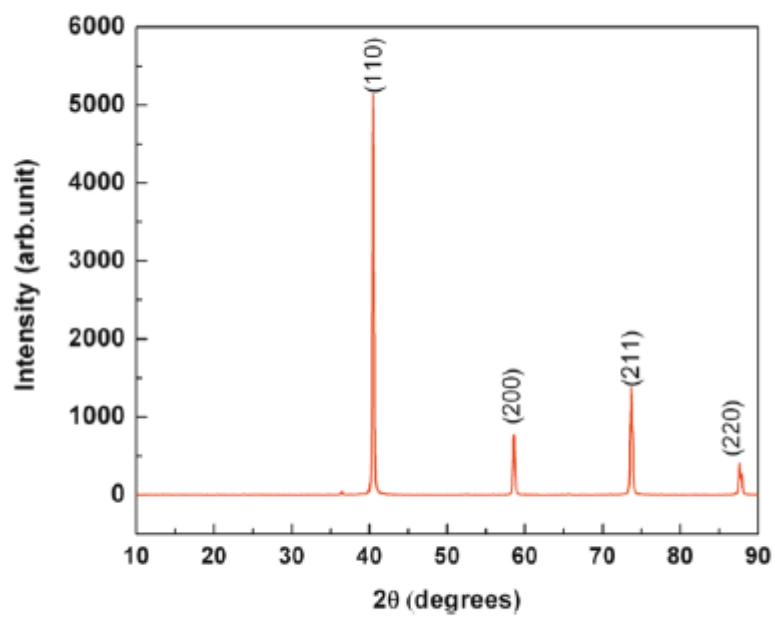


Figure 2

ACCEPTED

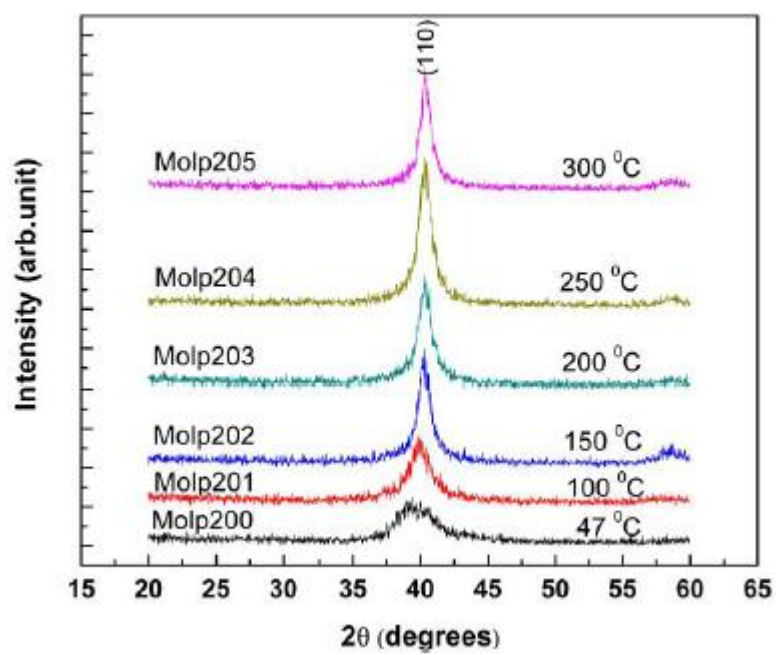


Figure 3

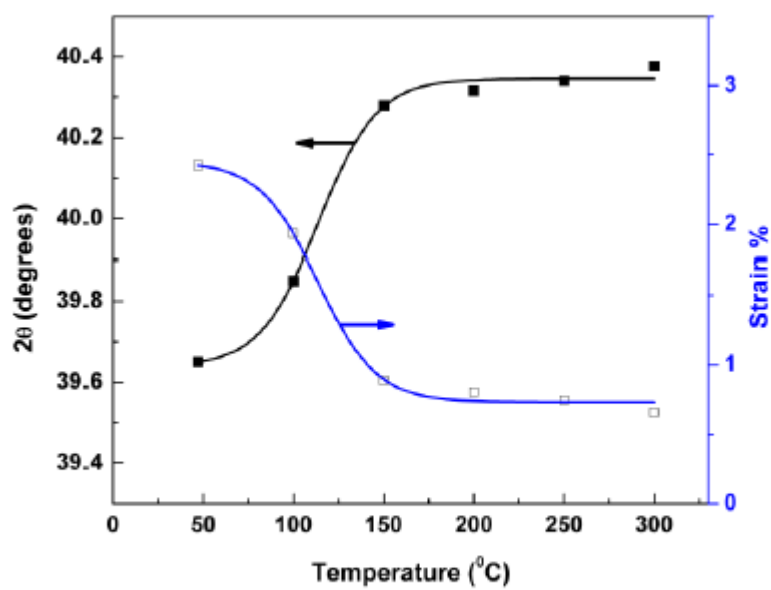


Figure 4

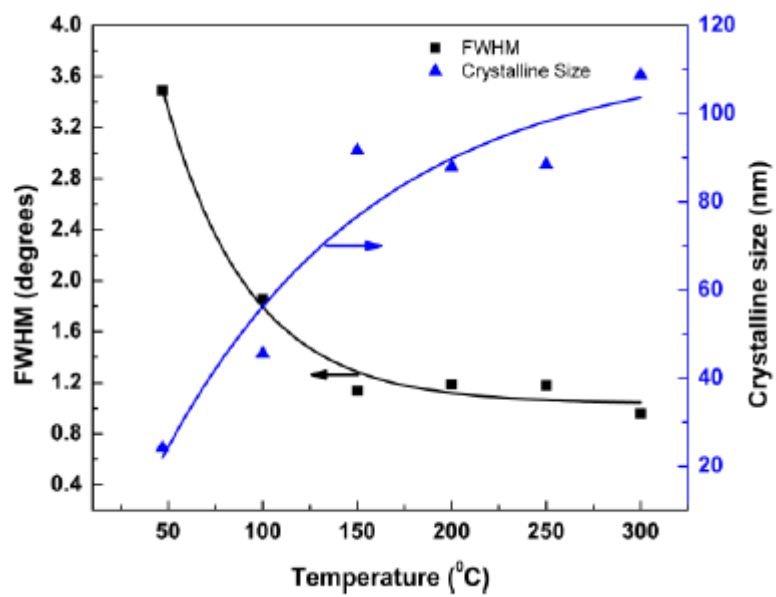


Figure 5

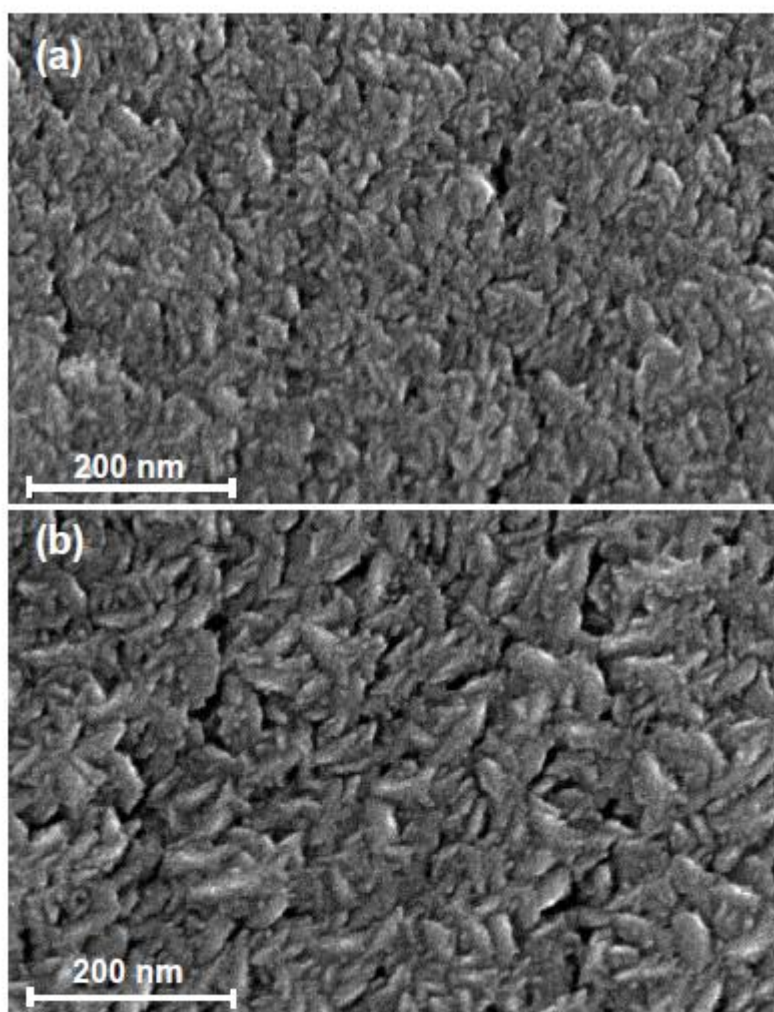


Figure 6

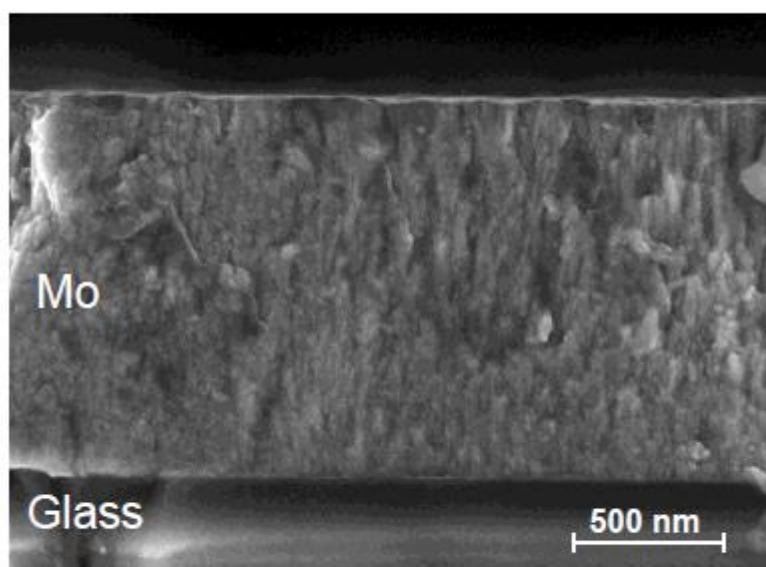


Figure 7

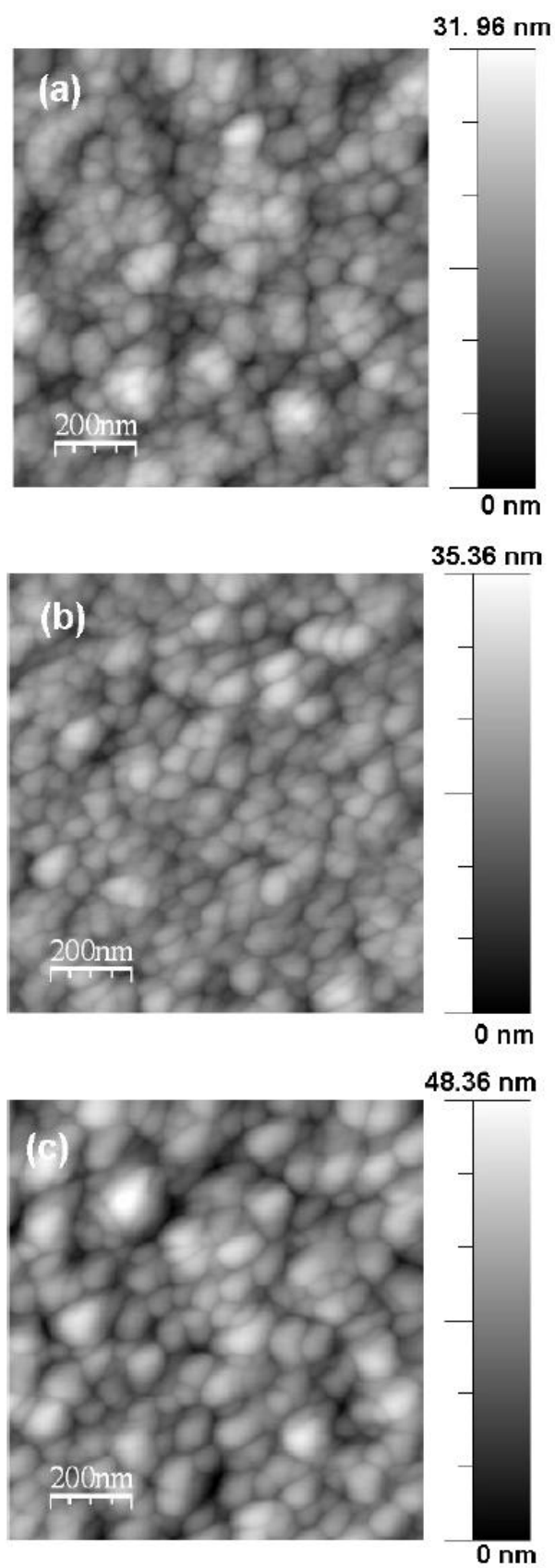


Figure 8

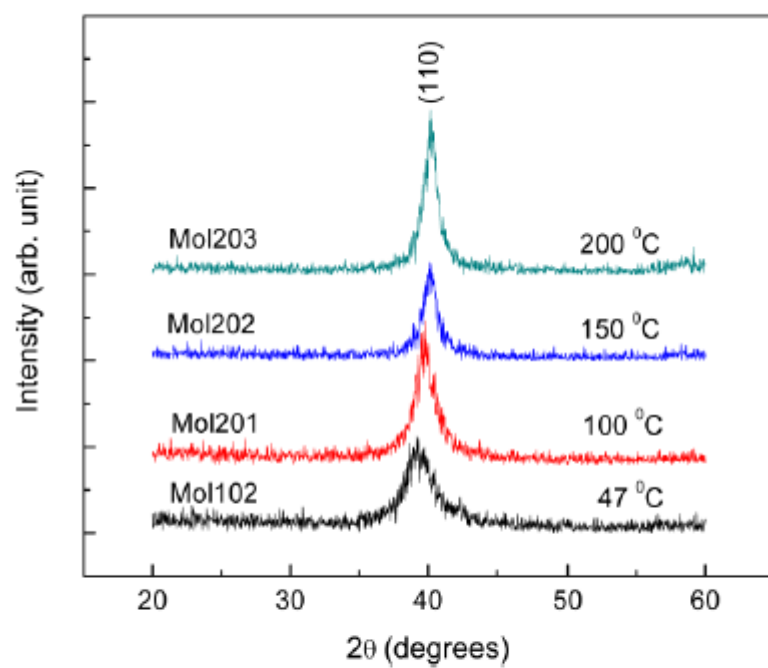


Figure 9

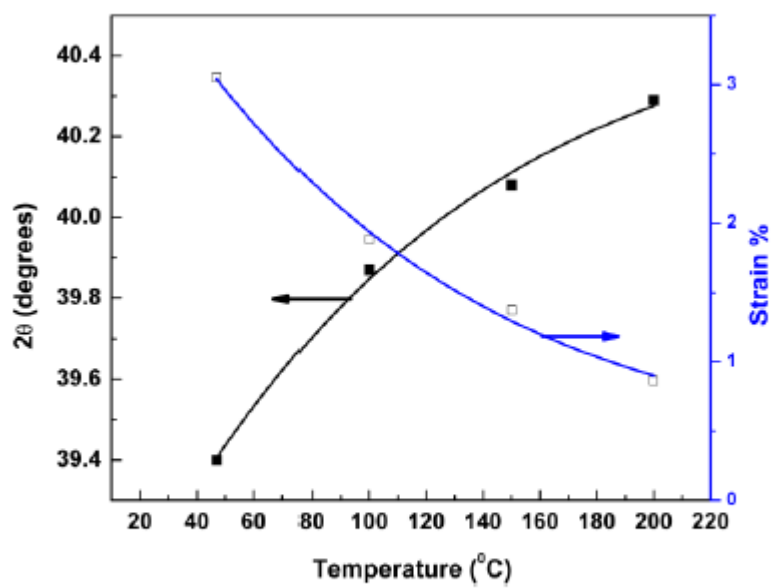


Figure 10